A NEW APPROACH TO TREAT THE RANS-LES INTERFACE IN PANS

Lars Davidson[1]

[1] *Div. of Fluid Dynamics, Dept. of Applied Mechanics*
Chalmers University of Technology, SE-412 96 Gothenburg

lada@chalmers.se

Abstract

The partially averaged Navier-Stokes (PANS) model, proposed by [1], can be used to stimulate turbulent flows either as a RANS, LES or DNS.

In [2], a method was proposed to include the effect of the gradient of f_k. This approach is used at RANS-LES interface in the present study. Three different interface models are evaluated in fully developed channel flow and embedded LES of channel flow.

The importance of the location of the interface in fully developed channel flow is also investigated. It is found that the location – and the choice of the treatment at the interface – may be critical at low Reynolds number. The reason is that the turbulent viscosity, in outer scaling, is larger – and hence the relative strength of the resolved turbulence is smaller – at low Reynolds numbers.

In RANS, the turbulent viscosity – and hence the modeled Reynolds shear stress – is only weakly dependent on Reynolds number. It is found that in the present work that also applies in the URANS region.

1 Introduction

Wall-bounded Large Eddy Simulation (LES) is affordable only at low Reynolds number. At high Reynolds number, the LES must be combined with a URANS treatment of the near-wall flow region. There are different methods for bridging this problem such as Detached Eddy Simulation (DES), hybrid LES/RANS and Scale-Adapted Simulations (SAS); for a review, see [3]. The two first classes of models take the SGS length scale from the cell size whereas the last (SAS) involves the von Kármán lengthscale.

In the present work, the PANS model is used as a zonal hybrid LES/RANS model to simulate wall-bounded flow at high Reynolds number. $f_k = 1$ in the near-wall region, and $f_k = 0.4$ in the LES region. The interface between the RANS and LES regions is defined along a grid line, an approach also chosen in ZDES [4]. As an alternative to using a constant f_k in the LES region, f_k can be computed using the cell size and the integral length scale, $k_{tot}^{3/2}/\varepsilon$ [5], where k_{tot} is the sum of the resolved and the modeled turbulent kinetic energy, i.e. $k_{tot} = k_{res} + k$. The reason why f_k is not computed is that it has been shown that a constant $f_k = 0.4$ works well in the LES region [6]; it was even shown in [6] that using constant $f_k = 0.4$ works better than computing f_k, not to mention that it is numerically more stable. It was furthermore shown that the k and ε equations in the LES region are both in local equilibrium (the time-averaged equations, not instantaneously, see Section 2).

In [2], a method was proposed to include the effect of the gradient of f_k. This may be important, for example, at RANS-LES interfaces. This approach is further developed in the present study. It is evaluated in fully developed channel flow and embedded LES of channel flow. in all cases, PANS is used as a zonal model. In fully developed channel flow, the RANS-LES interface is parallel to the wall and in embedded LES it is parallel to the inlet.

When the RANS-LES interface is parallel to the wall, the term including the gradient of f_k across the interface can be both positive and negative (because v' is both positive and negative). This term is included only when it reduces the modeled turbulence. Hence, the term can be seen as a *forcing* term which represents backscatter. It is used to stimulate growth of the resolved turbulence in the LES region adjacent to the RANS region. The present method reduces the gray area problem described in [7].

The paper is organized as follows. The next section describes the equations and the interface models. The following section describes the numerical method, followed by a section which presents and discusses the results. The final section presents the conclusions.

2 The PANS Model

The low-Reynolds number partially averaged Navier-Stokes (LRN PANS) turbulence model reads [8]

$$\frac{Dk}{Dt} = \frac{\partial}{\partial x_j}\left[\left(\nu + \frac{\nu_t}{\sigma_{ku}}\right)\frac{\partial k}{\partial x_j}\right] + P_k + P_{k_{tr}} - \varepsilon \quad (1)$$

$$\frac{D\varepsilon}{Dt} = \frac{\partial}{\partial x_j}\left[\left(\nu + \frac{\nu_t}{\sigma_{\varepsilon u}}\right)\frac{\partial \varepsilon}{\partial x_j}\right] + C_{\varepsilon 1} P_k \frac{\varepsilon}{k} - C^*_{\varepsilon 2}\frac{\varepsilon^2}{k}$$

where $D/Dt = \partial/\partial t + \bar{v}_j \partial/\partial x_j$ denotes the material derivative. The constants and damping functions are given in [8]. The term $P_{k_{tr}}$ is an additional term which is non-zero in the interface region because

$Df_k/Dt \neq 0$. The function f_ε, the ratio of the modeled to the total dissipation, is set to one since the turbulent Reynolds number is high. f_k is set to 1 in the RANS region and to 0.4 in the LES region. Attempts were made to compute f_k in the LES region, but because of the large gradient of f_k across the interface the simulations diverged. Furthermore, it has been found that in zonal RANS-LES $f_k = 0.4$ in the LES region is a suitable choice [6].

It was shown in [6] that the k and ε equations in the LES region are in local equilibrium, i.e.

$$\langle P_k \rangle - \langle \varepsilon \rangle = 0 \tag{2}$$

$$\left\langle C_{\varepsilon 1} \frac{\varepsilon}{k} P_k \right\rangle - \left\langle C^*_{\varepsilon 2} \frac{\varepsilon^2}{k} \right\rangle = 0 \tag{3}$$

It seems that Eqs. 2 and 3 cannot both be satisfied since $C_{\varepsilon 1} \neq C^*_{\varepsilon 2}$; indeed, the equations are not satisfied instantaneously for which the convective terms play an important role. Equation 3 is satisfied but

$$C_{\varepsilon 1} \frac{\langle \varepsilon \rangle}{\langle k \rangle} \langle P_k \rangle - C^*_{\varepsilon 2} \frac{\langle \varepsilon^2 \rangle}{\langle k \rangle} \neq 0. \tag{4}$$

Equations 2 and 3 are both satisfied because the correlation between ε, k^{-1} and P_k (left side of Eq. 3) is stronger than that between ε^2 and k^{-1} (right side). The correlation between the quantities on the left side is larger than that on the right side because $C^*_{\varepsilon 2} > C_{\varepsilon 1}$.

The Interface Condition

The commutation error in PANS was recently addressed in [2]. In PANS, the equation for the modeled turbulent kinetic energy, k, is derived by multiplying the k_{tot} equation ($k_{tot} = k_{res} + k$) by f_k. The convective term in the k equation with constant f_k is then obtained as

$$f_k \frac{Dk_{tot}}{Dt} = \frac{D(f_k k_{tot})}{Dt} = \frac{Dk}{Dt} \tag{5}$$

where

$$f_k = \frac{k}{k_{tot}}. \tag{6}$$

Now, if f_k varies in space, we get instead

$$\begin{aligned} f_k \frac{Dk_{tot}}{Dt} &= \frac{D(f_k k_{tot})}{Dt} - k_{tot} \frac{Df_k}{Dt} \\ &= \frac{Dk}{Dt} - k_{tot} \frac{Df_k}{Dt} \end{aligned} \tag{7}$$

The second term on the right side (excluding the minus sign) represents energy transfer from resolved to modeled turbulence. It can be written (on the right side of the k equation)

$$\begin{aligned} k_{tot} \frac{Df_k}{Dt} &= (k + k_{res}) \frac{Df_k}{Dt} \\ &= k \frac{Df_k}{Dt} + \frac{\bar{v}'_i \bar{v}'_i}{2} \frac{Df_k}{Dt} \end{aligned} \tag{8}$$

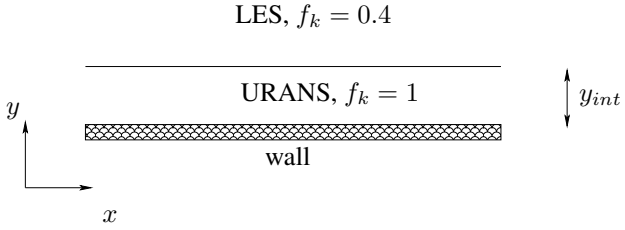

Figure 1: Fully developed channel flow. The URANS and the LES regions.

The second term on the right side can be represented by the source term

$$S^1_i = -0.5 \bar{v}'_i \frac{Df_k}{Dt} \tag{9}$$

in the momentum equation. Consider the momentum equation for the fluctuating velocity, $\bar{v}'_i$. Multiplying S^1_i by $\bar{v}'_i = \bar{v}_i - \langle \bar{v}_i \rangle$ and time-averaging gives the source term in the k_{res} equation as

$$-\left\langle (\bar{v}_i - \langle \bar{v}_i \rangle) \frac{\bar{v}'_i}{2} \frac{Df_k}{Dt} \right\rangle = -\left\langle \frac{\bar{v}'_i \bar{v}'_i}{2} \frac{Df_k}{Dt} \right\rangle \tag{10}$$

($\langle . \rangle$ denotes time averaging). Equation 10 is equal to the time average of the second term on the right side of Eq. 8 as it should. The signs in Eq. 10 and the right side of Eq. 8 are different because the former is part of the k_{res} equation whereas the latter is part of the k equation.

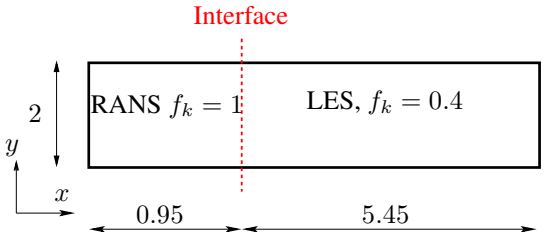

Figure 2: Embedded LES of channel flow.

The first term on the right side of Eq. 8 can be rewritten as

$$k \frac{Df_k}{Dt} = \frac{k \langle \bar{v}'_i \bar{v}'_i \rangle}{\langle \bar{v}'_m \bar{v}'_m \rangle} \frac{Df_k}{Dt} \tag{11}$$

A corresponding term can be added as a source term in the momentum equation as

$$S^2_i = -\frac{k \bar{v}'_i}{\langle \bar{v}'_m \bar{v}'_m \rangle} \frac{Df_k}{Dt} \tag{12}$$

Multiplying S^2_i by $\bar{v}'_i$ and time averaging gives

$$-\frac{\langle k \bar{v}'_i \bar{v}'_i \rangle}{\langle \bar{v}'_m \bar{v}'_m \rangle} \frac{Df_k}{Dt} \simeq -\langle k \rangle \frac{Df_k}{Dt} \tag{13}$$

where we assume that the correlation between k and $\bar{v}'_i$ is weak. Equation 13 is equal to (minus) the time

average of the first term on the right side of Eq. 8 as it should.

In [2], the second term on the right side of Eq. 7 is represented by introducing an additional turbulent viscosity, ν_{tr}, in a diffusion term in the momentum equation as

$$\frac{\partial}{\partial x_j}\left(\nu_{tr}\bar{s}_{ij}\right), \quad \bar{s}_{ij} = \frac{1}{2}\left(\frac{\partial \bar{v}_i}{\partial x_j} + \frac{\partial \bar{v}_j}{\partial x_i}\right) \tag{14}$$

where

$$\begin{aligned} \nu_{tr} &= \frac{P_{k_{tr}}}{|\bar{s}|^2}, \quad P_{k_{tr}} = 2\nu_{tr}\bar{s}_{ij}\bar{s}_{ij} \\ &= \nu_{tr}|\bar{s}|^2 = k_{tot}\frac{Df_k}{Dt} \end{aligned} \tag{15}$$

where the right side corresponds to the left side of Eq. 8. $P_{k_{tr}}$ is an additional production term in the k equation, see Eq. 1. In [2], $P_{k_{tr}}$ is re-written using Eq. 6 as

$$P_{k_{tr}} = \frac{k}{f_k}\frac{Df_k}{Dt} \tag{16}$$

Modeling the Interface

The gradient of f_k across a RANS-LES interface gives rise to an additional term in the momentum equations and the k equation. In the present work, these terms are included only when the flow goes from a RANS region to an LES region. The effect of these terms will reduce k and act as a forcing term in the momentum equations. Four different models are investigated.

Interface Model 1.

This is based on the approach suggested in [2]. The additional turbulent viscosity, ν_{tr}, gives an additional production term, $P_{k_{tr}}$, in the k equation, see Eq. 16. Since we are interested in stimulating resolved turbulence in the LES region adjacent to the RANS region, only negative values of ν_{tr} are included (i.e. $Df_k/Dt < 0$; this corresponds to a fluid particle in a RANS region passing the interface into an adjacent LES region). However, ν_{tr} takes such large (negative) values that $\nu_t + \nu_{tr} < 0$. To stabilize the simulations, it was found necessary to introduce a limit $\nu_t + \nu_{tr} > 0$ in the diffusion term in the momentum equation. No such limit is used in the k equation, and hence $P_k + P_{k_{tr}}$ is allowed to go negative.

Interface Model 2.

This model is identical to Model 1 except that Eq. 15 is used instead of Eq. 16. k_{tot} is defined as

$$k_{tot} = k + \frac{1}{2}\langle \bar{v}_i'\bar{v}_i' \rangle_{r.a} \tag{17}$$

where subscript $r.a.$ denotes running average. Since k_{tot} is mostly larger than k/f_k [6], this approach will give a larger magnitude of the (negative) production. It will be seen that this modification is of utmost importance.

Interface Model 3.

The right side of Eq. 8 is added to the k equation, but only when the flow goes from a RANS region to an LES region (i.e. $Df_k/Dt < 0$)

$$P_{k_{tr}} = k_{tot}\min\left(\frac{Df_k}{Dt}, 0\right) \tag{18}$$

where k_{tot} is computed as in Eq. 17. The production term $P_{k_{tr}} < 0$ which means that it reduces k as it should. The sum of the S_i^1 and S_i^2 terms (see Eqs. 9 and 12) in the momentum equations read

$$S_i = -\min\left(\frac{Df_k}{Dt}, 0\right)\left(0.5 + \frac{k}{\langle \bar{v}_m'\bar{v}_m' \rangle_{r.a.}}\right)\bar{v}_i' \tag{19}$$

Since $Df_k/Dt < 0$, the source S_i has the same sign as $\bar{v}_i'$; this means that the source enhances the resolved turbulence as it should.

It is however found that the forcing becomes too strong when S_i is added to the momentum equation. In the present work $S_i = 0$. The differences between Models 3 and 2 are that

- No explicit modification is made in the momentum equation in Model 3
- Model 2 (and Model 1) may need regularization in case $|\bar{s}| \to 0$ in the denominator of $\nu_{t_{tr}}$ in Eq. 15. No such regularization, however, is used in the present work.

Interface Model 4.

This interface model was developed in [6] for horizontal interfaces. The modeled turbulent kinetic energy in the LES region adjacent to the interface is reduced by setting the usual convection and diffusion fluxes of k at the interface to zero. New fluxes are introduced in which the interface condition is set to $k_{int} = f_k k_{RANS}$ ($f_k = 0.4$), where k_{RANS} is the k value in the cell located in the URANS region adjacent to the interface. No modification is made for the convection and diffusion of ε across the interface. For greater detail, see [6].

The treatment of the k equation for a vertical interface (the embedded interface in the channel flow) is exactly the same as for a horizontal interface. The difference is that an interface condition is needed also for the ε equation which reads [10]

$$\begin{aligned} \varepsilon_I &= C_\mu^{3/4}\frac{k_I^{3/2}}{\ell_{sgs}}, \quad \Delta = V^{1/3}, C_S = 0.1, \\ \ell_{sgs} &= C_S\Delta\varepsilon_I = C_\mu^{3/4} \end{aligned} \tag{20}$$

where subscript I denotes inlet or interface; V is the volume of the cell.

3 Numerical Method

An incompressible, finite volume code is used. The numerical procedure is based on an implicit, fractional step technique with a multigrid pressure Poisson solver and a non-staggered grid arrangement. For

Re_τ	Δy^+	Δx^+	Δz^+	N_y	f_y
2 000	$2.0 - 230$	200	100	80	1.13
4 000	$2.2 - 520$	400	200	80	1.15
8 000	$1.5 - 1\,050$	800	400	96	1.15

Table 1: Grids. Fully developed channel flow. f_y denotes geometric stretching.

the momentum equations, second-order central differencing is used for the fully developed channel flow. For the embedded channel flow, we use the second-order upwind van Leer scheme in the RANS region upstream of the interface and second-order central differencing in the LES region downstream of the interface. The Crank-Nicolson scheme is used in the time domain and the first-order hybrid central/upwind scheme is used in space for solving the k and ε equations.

4 Results

Fully Developed Channel Flow

The Reynolds number $Re_\tau = u_\tau \delta/\nu$ where δ denotes half channel height. Simulations at different Reynolds numbers are made, $Re = 2\,000$, $Re = 4\,000$ and $Re = 8\,000$. The streamwise, wall-normal and spanwise directions are denoted by x, y and z, respectively. The size of the domain is $x_{max} = 3.2$, $y_{max} = 2$ and $z_{max} = 1.6$. The mesh has 32×32 cells in the $x - z$ planes. A simulation with twice as large domain in the $x - z$ plane ($x_{max} = 6.4$ and $z_{max} = 3.2$) with 64×64 cells was also made for $Re_\tau = 4\,000$, and identical results were obtained as for the smaller domain. Details of the grids are given in Table 1. The baseline value for the location of the interface is $y^+ \simeq 500$.

Figure 3 presents the velocity profiles, the turbulent viscosities, the shear stresses and the production terms in the k equation. The vertical thick dashed lines show the location of the interface. Model 2 and 3 gives a velocity profile in good agreement with the log-law. Model 1 does not sufficiently reduce the turbulent viscosity in the LES region and the result is that the turbulent viscosity is much too large but somewhat smaller than "no interface condition". With Model 2, the magnitude of the additional turbulent viscosity near the interface is actually larger than ν_t, which makes their sum, $\nu_t + \nu_{tr}$, go negative. Please recall that in the momentum equations $\nu_t + \nu_{t_{tr}}$ is not allowed to go negative; it is negative only in $P_{k_{tr}}$, see Section 2. As a consequence of the large, negative $\nu_{t_{tr}}$, $P_k + P_{k_{tr}} < 0$ at the interface. The shear stresses in Fig. 3d show that without interface condition the flow goes steady. Note that to enhance the readability of the figure, the negative viscous plus modeled shear stresses, $-\tau_{12}^\nu - \tau_{12}$, are plotted. Recall that the total shear stress, τ_{tot}, will

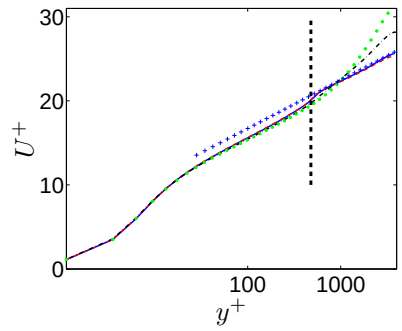

(a) Velocity. $+$: $U^+ = \ln(y^+)/0.4 + 5.2$

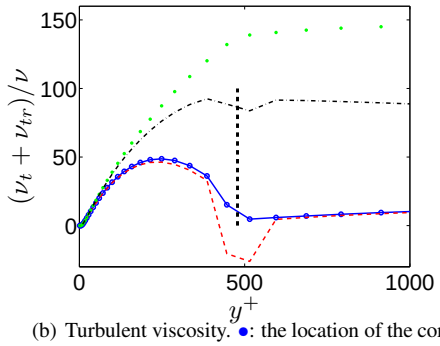

(b) Turbulent viscosity. $\bullet$: the location of the computational cell centers.

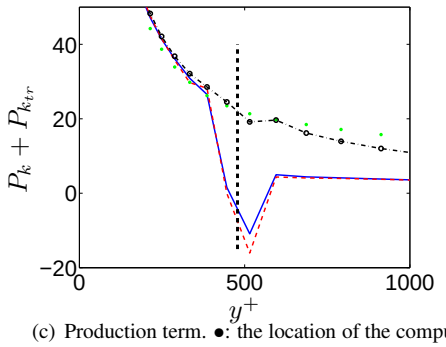

(c) Production term. $\bullet$: the location of the computational cell centers.

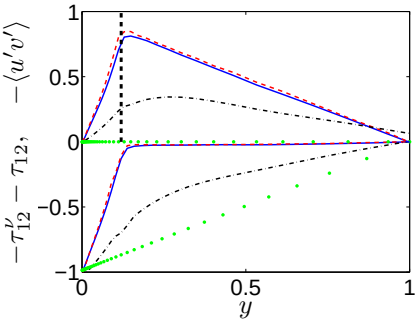

(d) Resolved (upper lines) and viscous plus modeled (lower) shear stresses.

Figure 3: Fully developed channel flow. $Re_\tau = 4\,000$. ▬ ▬ : Model 1. ▬ ▬ : Model 2. ▬ : Model 3; ▬ ▬ : no interface condition.

always – irrespectively of model – obey the linear law

$$\begin{aligned} \tau_{tot} &= 1 - y, \quad \tau_{tot} = \tau_{12}^\nu + \tau_{12} - \langle u'v' \rangle \\ &= \langle (\nu + \nu_t) \frac{\partial \bar{v}}{\partial y} - u'v' \rangle \end{aligned} \tag{21}$$

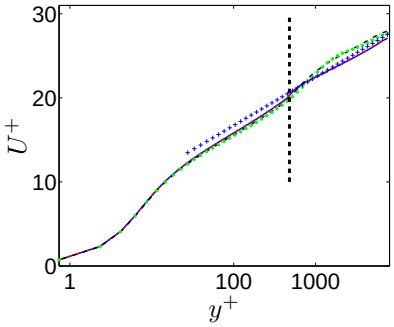

(a) Velocity. +: $U^+ = \ln(y^+)/0.4 + 5.2$

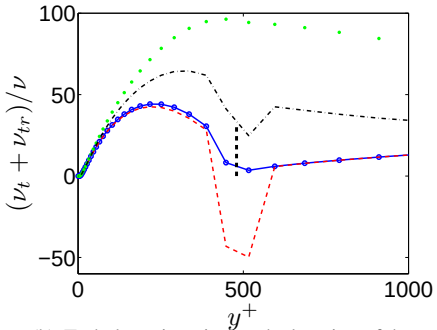

(b) Turbulent viscosity. •: the location of the computational cell centers.

Figure 4: Fully developed channel flow. $Re_\tau = 8\,000$. For legend, see Fig. 3.

With Model 1 the flow is neither in RANS mode nor in LES mode, but it ends up in being in the middle, which is a most unfortunate condition for a hybrid LES-RANS model. The stresses predicted by Models 2 and 3 are virtually identical.

Figure 4 shows the same quantities as Fig. 3, but now for $Re_\tau = 8\,000$. Again, Models 2 and 3 give good velocity profiles. Model 1 and the "no interface condition" give rather good velocity profiles although the velocity is somewhat too high in the LES region. The reason for the larger velocity levels is seen in Fig. 4b which presents the turbulent viscosities. The "no interface condition" does not manage to reduce ν_t in the LES region; also Model 1 is much less efficient in reducing ν_t than are Models 2 and 3.

Models 1–3 fail for $Re_\tau = 2\,000$ (not shown). In order to find the reason for this failure, the sensitivity to the location of the interface was investigated. Figure 5 presents the velocities, turbulent viscosities and the shear stresses using Model 4 for $Re_\tau = 2\,000$, $4\,000$ and $8\,000$ for different locations of the interface. The velocity profiles are well predicted for all cases expect for $Re_\tau = 8\,000$ and $y^+_{interface} = 250$. Note that the turbulent viscosities are plotted using outer scaling (i.e. they are scaled with friction velocity, u_τ, and half channel width, δ). The results from a one-dimensional RANS simulation using the AKN model (i.e. PANS with $f_k = 1$) are also included. When plotted versus y, the RANS turbulent viscosity is virtually independent of Reynolds number and hence all

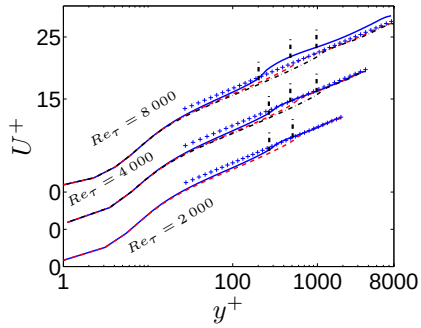

(a) Velocity. +: $U^+ = \ln(y^+)/0.4 + 5.2$

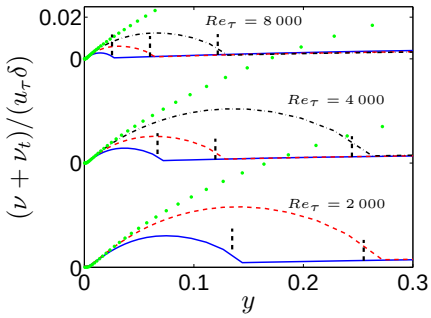

(b) Viscosity

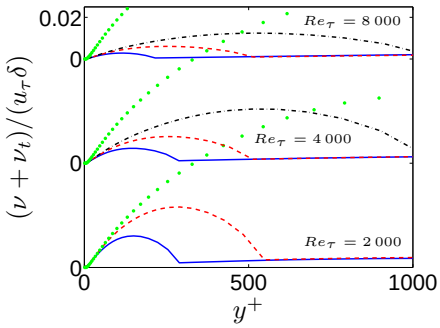

(c) Viscosity

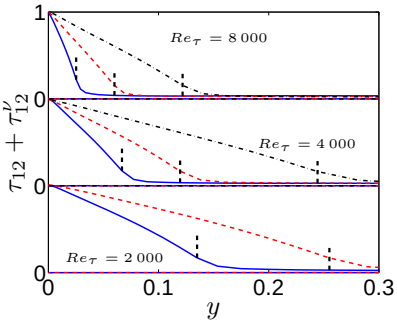

(d) Viscous plus modeled shear stress

Figure 5: Fully developed channel flow. Model 4. $Re_\tau = 2\,000$ (lower lines), $Re_\tau = 4\,000$ (middle lines), and $Re_\tau = 8\,000$ (upper lines). Vertical dashed thick lines show the location of the interfaces. ——: $y^+_{interface} = 250$; - - -: $y^+_{interface} = 500$; — - —: $y^+_{interface} = 1\,000$; · · ·: 1D RANS using AKN model.

the green dotted lines in Fig. 5c are the same. Actually this is also the case for the PANS simulations when the interface is defined in outer scaling (i.e. in y): in Fig. 5b, the turbulent viscosity in the URANS region for

- $\{Re_\tau = 2\,000,\ y^+_{interface} = 250\}$, and $\{Re_\tau = 4\,000,\ y^+_{interface} = 500\}$ and $\{Re_\tau = 8\,000,\ y^+_{interface} = 1\,000\}$ (i.e. $y = 0.125$)
- $\{Re_\tau = 2\,000,\ y^+_{interface} = 500\}$, and $\{Re_\tau = 4\,000,\ y^+_{interface} = 1\,000\}$ (i.e. $y = 0.25$)

are very similar. As a result, this applies also for the viscous plus modeled shear stresses, see Fig. 5d. It is interesting to note that the viscosity in the RANS region in the PANS simulations is much smaller than that in the 1D RANS simulation. The reason is, as noted in [6], that low modeled k is transported from the LES region into the RANS region near the lower wall when $v' < 0$ (ε in the LES region in the two simulations are very similar, see [6]).

Now we need to address the question why Models 1-3 fail at $Re_\tau = 2\,000$. The interface location was moved away from the wall to $y^+_{interface} \simeq 1000$, but the same results were obtained (not shown). Next, the interface location was moved closer to the wall, to $y^+_{interface} \simeq 250$. Model 1-3 still fail to predict a good velocity profile (not shown). It was mentioned above that the reason for the poor prediction of the velocity profile at $Re_\tau = 2\,000$ could be that the resolved shear stress is too low at the interface, and that the low level of resolved turbulence in the interface region would make the transition from RANS mode to LES mode difficult. However, this theory does not hold when we look at the resolved shear stresses at the interface at $Re_\tau = 2\,000$ (not shown) which are as large or larger than those at $Re_\tau = 8\,000$ for which good velocity profiles are obtained. The reason for the poor prediction at $Re_\tau = 2\,000$ is that the turbulent viscosity (in outer scaling) is much larger than at the higher Reynolds number, see Figure 5b,c. Because of this, Models 1-3 do not manage to sufficiently decrease ν_t in the LES region adjacent to the interface.

Embedded LES of Channel Flow

The Reynolds number is $Re_\tau = u_\tau \delta/\nu = 950$. The domain size is $6.4 \times 2 \times 1.6$ in the streamwise (x), wall-normal (y) and spanwise direction (z), see Fig. 2. The mesh has $128 \times 80 \times 64$ cells. A geometrical stretching of 1.13 in the y direction is used from the walls to the center. Anisotropic fluctuations are added to the momentum equations at the interface [11, 10]. The time-averaged interface fluctuations and the two-point correlation of w' are shown in Fig. 6. As can be seen, a constant amplitude is used across the channel. The reason for this choice instead of making the Reynolds stresses vary across the channel is that it is simpler and it was found in [11] to be more efficient in stimulating the growth of resolved fluctuations. It

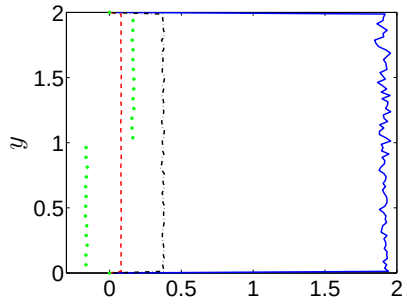

(a) Reynolds stresses.

Figure 6: Embedded LES. Prescribed synthetic Reynolds stresses at the vertical RANS-LES interface. ——: u^2_{rms}/u^2_τ; - - -: v^2_{rms}/u^2_τ; – – –: w^2_{rms}/u^2_τ; ·····: $\langle u'v'\rangle/u^2_\tau$.

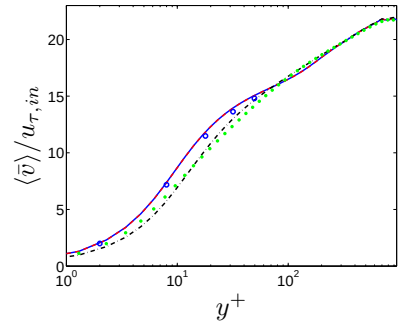

(a) Velocity.

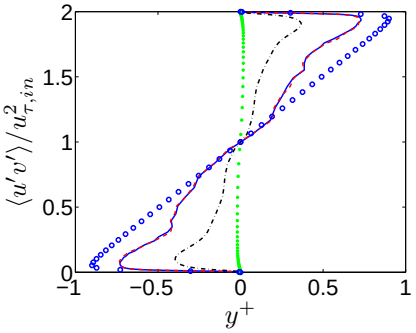

(b) Resolved shear stress

Figure 7: Embedded LES. $Re_\tau = 950$. $x = 5.9$. For legend, see Fig. 3.

can be noted in Fig. 6 that the sign of the shear stress changes at the centerline. This was achieved by simply switching the sign of the vertical synthetic fluctuation, v', for $y > 1$. When creating the synthetic turbulent interface fluctuations, the length scale was set to 0.15. Figure 6b shows that the two-point correlation of the generated fluctuations agrees well with this value. A Matlab file to generate the synthetic fluctuations can be downloaded at [12]. RANS is used upstream of the interface ($f_k = 1$) and LES is used downstream of it ($f_k = 0.4$). Models 1-3 are used at the vertical interface. Model 4 was used in [10] and was found to work well.

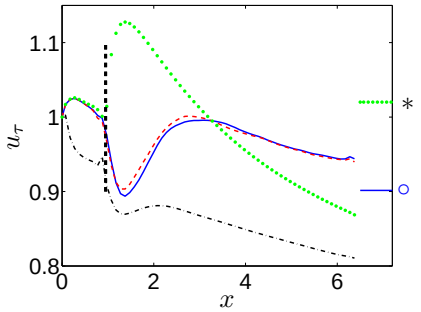

(a) Friction velocity. $*$: u_τ, RANS for fully-developed channel; $\circ$: u_τ, PANS for fully-developed channel.

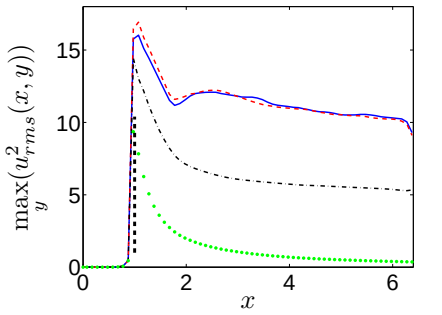

(b) Streamwise fluctuations

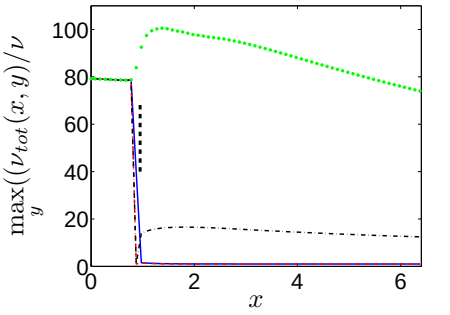

(c) Turbulent viscosities. $\nu_{tot} = \nu + \nu_t + \nu_{tr}$.

Figure 8: Embedded LES. $Re_\tau = 950$. Vertical thick dashed lines show the RANS-LES interface. For legend, see Fig. 3.

Figures 7 and 8 present velocity profiles, resolved turbulence, skin friction, turbulent viscosity and production of modeled turbulent kinetic energy. First, it can be noted that without any interface model, little resolved turbulence survives in the LES region because it is killed by the large turbulent viscosity. Also Model 1 does not reduce the turbulent viscosity sufficiently, although it is not as bad as the "no interface model". For Model 1, some resolved turbulence survives but it is small. The friction velocity (Fig. 8a) is the most critical parameter. At the right of the figure, the fully-developed values for PANS and RANS are indicated. As can be seen, Models 2 and 3 give actually much better value of u_τ (the target value is one) than the fully-developed values; for a very long channel, however, the u_τ values will approach the values indicated at the right. Models 2 and 3 give $u_\tau \simeq 1$ already two half-channel heights downstream of the interface, which is quite good. The resolved turbulence is fairly good near the wall, but it will take some time (i.e. streamwise distance) to reach their fully-developed profiles; the resolved shear stress (Fig. 7b) – which is the most important – is fairly well developed. The profiles of the normal resolved stresses still remember the constant profiles imposed at the interface (not shown). But, as mentioned above, the advantage of using a constant imposed interface profiles is that it is very efficient in creating resolved turbulence. In the case of Model 1, the resolved turbulence further downstream ($x \gg 6.4$) will probably first be completely killed and then the flow will eventually go into RANS mode. With Models 2 and 3, the resolved turbulence at the interface increases strongly (Fig. 8b) thanks to the added non-isotropic fluctuations, but also thanks to interface conditions of Models 2 and 3 which succeed in drastically decreasing the modeled turbulent kinetic energy and thereby the turbulent viscosity, see Fig. 8c. The turbulent viscosity is actually completely killed for $x \gtrsim 2$. The turbulent viscosity is reduced already upstream of the interface because $\partial f_k/\partial x < 0$ at the computational cell upstream of the interface. The turbulent viscosity with Model 3 is reduced one cell further downstream compared to Models 1 and 2. The reason is that Model 3 does not modify the turbulent viscosity in the momentum equations, but it modifies only the production, P_k, by adding $P_{t_{tr}}$. Models 1 and 2 modify the turbulent viscosity by adding $\nu_{t_{tr}}$ in the momentum equations (they modify also production through $\nu_{t_{tr}}$). Careful inspection of Fig. 8c shows that Model 1 does indeed reduce ν_t at the interface, but – contrary to Model 2 – the turbulent viscosity increases directly downstream of it. The reason is that Model 2 creates much larger negative $\nu_{t_{tr}}$ than does Model 1; for Model 2 $\max(-\nu_{t_{tr}})/\nu \simeq 300$ and for Model 1 $\max(-\nu_{t_{tr}})/\nu \simeq 150$. For Model 2 the maximum is located in the computational cell downstream of the interface because $k_{tot} = k + k_{res}$ (see Eq. 15) is largest here. Upstream of the interface, Model 2 gives $\max(-\nu_{t_{tr}})/\nu \simeq 190$.

As for the fully-developed channel flow, it is found that the productions by the interface models, $P_{k_{tr}}$, are very large and negative for Models 2 and 3 (not shown). These large negative productions ensure the strong decrease in turbulent viscosity across the RANS-LES interface, see Fig. 8c, which in turn facilitates the rapid increase in resolved turbulence downstream of the interface, see Fig. 8b.

5 Conclusions

Simulations using Zonal PANS are made where $f_k = 1$ in the URANS regions and $f_k = 0.4$ in the LES regions. There is a a strong gradient of f_k across the RANS-LES interface. Recently a modification of the PANS model was proposed by [2] where they take the gradient of f_k into account. This approach is used at the RANS-LES interfaces and it is further devel-

oped and evaluated in the present work. Four different treatments of the interface are evaluated, one is the approach proposed in [2] (called Model 1), Models 2 and 3 are modifications of Model 1 and Model 4 is the approach presented in [6]. The beauty of Models 1-3 is that they do not depend on any constants or tuning; they are given by the gradient of f_k across the interface. The disadvantage of Model 4 is that is depends on how the modeled k and ε are prescribed at the interface. The four models are evaluated in fully developed channel flow and embedded LES in channel flow.

Model 1 does not give good results. Its effect is too weak and the model does not sufficiently decrease the turbulent viscosity on the LES side of the interface. Models 2 and 3 give mostly good results and always virtually identical results. To make Models 1 and 2 numerically stable, the additional turbulent viscosity, $\nu_{t_{tr}}$, from the models must be positive in the momentum equations. In the production term in the k equation $\nu_{t_{tr}}$ is permitted to go negative. No modifications are made in the momentum equations in Model 3. The magnitude of the negative added production, $P_{k_{tr}}$, in the modeled k equation is very large, much larger than the ordinary P_k. This is the key to the success of Model 2 and 3; $P_{k_{tr}}$ is very large and negative in a few cells straddling the interface which reduces k and thereby the turbulent viscosity. Models 2 and 3 fail for the fully developed flow at the lowest Reynolds number ($Re_\tau = 2\,000$); they both give steady RANS results. Model 4 works well for all flows.

In fully developed channel flow using RANS, the turbulent viscosity, and hence the modeled Reynolds shear stress, is virtually independent of the Reynolds number. Using Zonal PANS, it is found that this also applies for the turbulent viscosity and the modeled Reynolds shear stress in the URANS region.

The conclusion is that interface Model 4 works best and that Models 2 and 3 fail in one flow (fully developed channel flow at $Re_\tau = 2\,000$). The disadvantage of Model 4 is that it depends on the prescribed boundary conditions of k and ε at the RANS-LES interface.

References

[1] S.S. Girimaji. Partially-Averaged Navier-Stokes model for turbulence: A Reynolds-averaged Navier-Stokes to direct numerical simulation bridging method. *Journal of Fluids Engineering*, 73(2):413–421, 2006.

[2] S. S. Girimaji and S. Wallin. Closure modeling in bridging regions of variable-resolution (VR) turbulence computations. *Journal of Turbulence*, 14(1):72 – 98, 2013.

[3] J. Fröhlich and D. von Terzi. Hybrid LES/RANS methods for the simulation of turbulent flows. *Progress in Aerospace*, 44(5):349–377, 2008.

[4] Sbastien Deck. Recent improvements in the zonal detached eddy simulation (zdes) formulation. *Theoretical and Computational Fluid Dynamics*, 26(6):523–550, 2012.

[5] B. Basara, S. Krajnović, S. Girimaji, and Z. Pavlović. Near-wall formulation of the Partially Averaged Navier Stokes turbulence model. *AIAA Journal*, 49(12):2627–2636, 2011.

[6] L. Davidson. The PANS $k-\varepsilon$ model in a zonal hybrid RANS-LES formulation. *International Journal of Heat and Fluid Flow*, pages 112–126, 2014.

[7] A. Travin, M. Shur, M., Strelets, and P. Spalart. Detached-eddy simulations past a circular cylinder. *Flow, Turbulence and Combustion*, 63:293–313, 2000.

[8] J. Ma, S.-H. Peng, L. Davidson, and F. Wang. A low Reynolds number variant of Partially-Averaged Navier-Stokes model for turbulence. *International Journal of Heat and Fluid Flow*, 32(3):652–669, 2011.

[9] H.K. Versteegh and W. Malalasekera. *An Introduction to Computational Fluid Dynamics - The Finite Volume Method*. Longman Scientific & Technical, Harlow, England, 1995.

[10] L. Davidson and S.-H. Peng. Embedded large-eddy simulation using the partially averaged Navier-Stokes model. *AIAA Journal*, 51(5):1066–1079, 2013.

[11] L. Davidson. Using isotropic synthetic fluctuations as inlet boundary conditions for unsteady simulations. *Advances and Applications in Fluid Mechanics*, 1(1):1–35, 2007.

[12] L. Davidson. How to implement synthetic inlet boundary conditions. http://www.tfd.chalmers.se/˜lada/projects/inlet-boundary-conditions/proright.html, 2013.